Spatial Coherence and Entanglement of Light

Di Lorenzo Pires, H.

8

Spatial coherence of partially coherent classical beams with and without orbital angular momentum

We study the spatial coherence of a partially coherent beam before and after being transmitted through a spiral phase plate that changes the overall orbital angular momentum of the field. The two-point coherence function is measured and directly visualized on a CCD through interference in a Mach-Zehnder interferometer equipped with an image rotator. We show, in particular, how the coherence singularities associated with Airy rings are strongly affected by the spiral phase plate.

H. Di Lorenzo Pires, J. Woudenberg, and M. P. van Exter, *Measurements of spatial coherence of partially coherent light with and without orbital angular momentum*, J. Opt. Soc. Am. A **27**, 2630 (2010).

8.1 Introduction

Coherent singular optics is a prominent field of optical sciences [138]. Since the pioneering paper of Nye and Berry [139], great effort has been devoted to understand the fundamental properties of the "dislocations in wave trains" and to develop its technological applications. Wave dislocations or phase singularities are singular points of a complex-valued function, like in the complex representation of the electric field, where the amplitude is zero and the phase not well defined. A prominent example of such singularities are the so-called optical vortices. They are present in coherent beams, like the Laguerre-Gauss modes, and are associated with a screw-like circulation of the phase around the center of the beam, where the intensity is zero [140]. Another example of phase singularities are the dark rings of an Airy pattern, which appears in the focal plane of a uniformly illuminated lens [141] or in the diffraction pattern of a spatially coherent wave behind a circular aperture [142, 143].

Recently, the field of singular optics was extended to the realm of partially coherent light and the concept of "phase singularities of correlation functions" was introduced [127, 128, 144, 145]. A partially coherent field can be mathematically described by its cross-spectral density function (or coherence function) $W(\mathbf{r}_1, \mathbf{r}_2)$, which determines how the fluctuations of the field at a certain point $\mathbf{r}_1$ are correlated with the fluctuations at $\mathbf{r}_2$. When a partially coherent beam is transmitted through an aperture or a spiral phase plate, sets of points can be found where the coherence is zero valued, implying the existence of phase singularities of this function. These points usually form a line in the transition between positively and negatively correlated field. The correlation singularity is considered a 'virtual' feature of the field, as it cannot be associated with any zeros of intensities but only with zeros of the two-point second-order coherence function [146].

This new branch of singular optics has been extensively studied, both theoretically [146–152] and experimentally [153–157]. Observations of a "coherence vortex" for an incoherent field have been reported [156] and the robustness of these singularities has been demonstrated [154]. The importance of correlation singularities to imaging science, where partially coherent illumination is often employed, has also been considered [150]. For a comprehensive discussion on the subject, see Ref. [158].

In this Chapter we will present measurements of the cross-spectral density $W(\mathbf{r}_1, \mathbf{r}_2)$ for partially coherent light that exhibits two types of coherence singularities. The first singularities are the Airy rings that appear in the coherence function upon propagation behind a circular aperture with incoherent illumination. The second type of singularities are created by the transmission through a spiral phase plate with topological charge $\ell = 1$. The field now acquires an overall orbital angular momentum $\ell\hbar$ per photon and an additional ring dislocation becomes visible in the coherence. We will show how these two types of singularities interact when the transverse coherence length of the source is changed.

In theoretical analyses of spatial correlation vortices in partially coherent

beams, the coherence of the initial field is often approximated by a Gaussian-Schell correlator [2], such that the input contains no coherence singularities. Although this approach allows analytical solutions, it can be an oversimplification of the experimental geometry. This remark also applies to [154], in which the existence of a ring dislocation in the correlation function was experimentally verified for the first time. In this Chapter we will develop a different theoretical approach that allows us to compute the propagation of a more general class of partially coherent fields, before and after being transmitted through a vortex phase plate.

Experimentally, we measure the cross-spectral density function of the field through interference in a Mach-Zehnder interferometer equipped with an image rotator. Furthermore, we implement a powerful method that allows the coherence singularities to be visualized in one single picture.

The Chapter is organized as follows: In Section 8.2 we formally introduce the cross-spectral density and calculate this function for our particular source. In Section 8.3 a convenient mathematical description of the propagation of partially coherent fields is developed and results of numerical simulations are presented. In section 8.4 we describe the experimental setup and present the results of our measurements. A summary of the results and conclusions are presented in Section 8.5.

8.2 Cross-spectral density

The state of coherence of light can be described by the cross-spectral density or mutual coherence function $W(\boldsymbol{\rho}_1, \boldsymbol{\rho}_2, z; \omega) = \langle E^*(\boldsymbol{\rho}_1, z; \omega) E(\boldsymbol{\rho}_2, z; \omega) \rangle$, where the brackets $\langle \cdots \rangle$ denotes average over an ensemble of strictly monochromatic waves. We are considering here the correlations between the transverse positions $\boldsymbol{\rho}_1$ and $\boldsymbol{\rho}_2$ at a fixed plane z. The cross spectral density can be measured by superposing the field with a phase delayed and spatially shifted copy of itself, yielding a combined intensity pattern profile

$$I = I_1 + I_2 + 2\mathrm{Re}\left[W(\boldsymbol{\rho}_1, \boldsymbol{\rho}_2, z; \omega) e^{i\delta}\right], \tag{8.1}$$

where I_1 and I_2 are the intensities at positions $\boldsymbol{\rho}_1$ and $\boldsymbol{\rho}_2$. By varying the phase δ and subtracting the single intensities, both the real and imaginary components of W can be obtained (see Sec. 4.7.2 of [2] for a more rigorous derivation). For simplicity, we will omit the frequency ω dependence in the derivation below of the cross-spectral density function for our particular source.

Figure 8.1 shows the geometry considered for the calculations. A circular aperture of diameter d_1 is uniformly illuminated by fully incoherent light. A second aperture of diameter d_2 is placed at a distance L from the first aperture, in a plane defined as $z = 0$. The field correlations between points $\boldsymbol{\rho}_1$ and $\boldsymbol{\rho}_2$ at $z = 0$ can be computed with the van Cittert-Zernike theorem [2], which states that the mutual coherence $W(\boldsymbol{\rho}_1, \boldsymbol{\rho}_2)$ in the far field of a spatially incoherent planar source is the Fourier transform of the intensity across the source. The cross-spectral density of the beam at $z = 0$, just behind aperture 2 is thus given

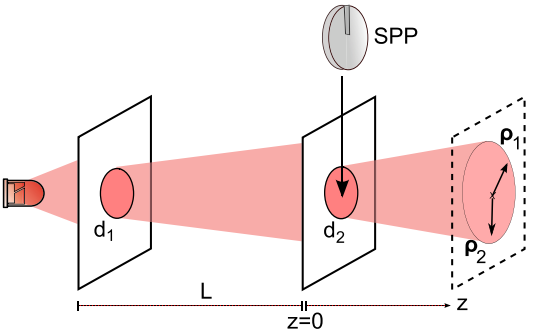

Figure 8.1: Geometry considered for the calculations. A circular aperture of diameter d_1 is illuminated by fully incoherent light. A second aperture of diameter d_2 is placed at a distance L from d_1, at $z = 0$. A spiral phase plate (SPP) can be placed just after aperture 2. The field correlations between the transverse positions $\boldsymbol{\rho}_1$ and $\boldsymbol{\rho}_2$ at the plane z are studied.

by

$$W_0(\boldsymbol{\rho_1}, \boldsymbol{\rho_2}) = T(\rho_1)T(\rho_2)\frac{J_1(\alpha|\boldsymbol{\rho_1} - \boldsymbol{\rho_2}|)}{\alpha|\boldsymbol{\rho_1} - \boldsymbol{\rho_2}|}e^{\frac{i\pi}{\lambda L}(\rho_1^2 - \rho_2^2)}, \tag{8.2}$$

where $J_1(\ )$ is the first order Bessel function of the first kind, $\alpha = \pi d_1/\lambda L$, and λ is the optical wavelength. The function $T(\rho)$ describes the intensity profile at $z = 0$. It describes both the transmission profile of the second aperture and the illuminating intensity profile at $z = 0$, which itself is determined by the coherence of the light in the source d_1. The intensity at $z = 0$ is uniform only in the limit of fully incoherent illumination [133].

The mutual coherence W_0 generally decreases at increased distance between the two points $\boldsymbol{\rho}_1$ and $\boldsymbol{\rho}_2$, up to a separation where the light is completely uncorrelated. This separation is defined as the coherence length L_c of the beam. Inspired by the theory of diffraction, the zeros of the function $J_1(x)/x$ are denoted as the coherence Airy rings. For the first Airy ring we have

$$L_c = 1.22\frac{\lambda L}{d_1}. \tag{8.3}$$

For a separation somewhat larger than L_c the coherence reappears. The fluctuations of the field are now slightly anti-correlated, associated with a π phase shift in the complex coherence function.

In order to investigate the properties of a coherence vortex, we add a spiral phase plate (SPP) centered inside aperture 2. This plate introduces a phase $e^{i\ell\phi}$ to the optical field, i.e., a phase factor that varies linearly with the azimuthal angle ϕ, and is able to change the overall angular momentum of the beam by $\ell\hbar$ per photon. If the incident field would be a coherent Gaussian beam, the output beam would acquire a dip in the intensity that goes to zero and has an increasing

width under propagation [159]. The effect of this same SSP on a *partially coherent* beam is to change the cross-spectral density according to

$$W(\boldsymbol{\rho}_1, \boldsymbol{\rho}_2) = W_0(\boldsymbol{\rho}_1, \boldsymbol{\rho}_2) e^{i\ell(\phi_1 - \phi_2)}, \tag{8.4}$$

where W_0 and W are the cross-spectral density just before and just after the SPP, respectively, and ϕ_i is the azimuthal angle corresponding to the transverse position vector $\boldsymbol{\rho}_i$, for $i = 1, 2$. Under partially coherent illumination, the intensity after the SSP doesn't go to zero anymore. The coherence function will, however, still exhibit a zero, i.e., a coherence vortex in the form of a ring dislocation whose radius increases as the beam propagates [154]. Part of this Chapter addresses the question: "What is combined effect of this vortex ring with the Airy rings already present in the incident beam?"

8.3 Propagation of a partially coherent beam

The theory of propagation of partially coherent beams is well known [2,4]. Since the mutual coherence function satisfies two independent wave equations for the two position coordinates, both coordinates can be independently propagated using the same propagation laws of fields. In the Fresnel regime, the propagation of the cross-spectral density $W(\boldsymbol{\rho}_1, \boldsymbol{\rho}_2; 0)$ from the plane $z = 0$ to a certain plane $z > 0$ can thus be written as

$$W(\boldsymbol{\rho}_1, \boldsymbol{\rho}_2; z) = \tag{8.5}$$
$$\iint_{-\infty}^{+\infty} W(\boldsymbol{\rho}_1', \boldsymbol{\rho}_2'; 0) e^{i\frac{k}{2z}|\boldsymbol{\rho}_1 - \boldsymbol{\rho}_1'|^2} e^{-i\frac{k}{2z}|\boldsymbol{\rho}_2 - \boldsymbol{\rho}_2'|^2} \, d\boldsymbol{\rho}_1' \, d\boldsymbol{\rho}_2',$$

where $k = 2\pi/\lambda$. Proportionality factors will be omitted in all equations throughout the Chapter. Equation (8.5) is a four-dimensional (4D) integral that cannot be easily solved, neither analytically nor numerically, except in a few special cases. Different approaches have been proposed in order to numerically treat this problem, such as the coherent-mode decomposition [2], Fourier-transform method [160], Monte Carlo simulation [161], and use of elementary functions [162]. One strategy is trying to rewrite Eq. (8.5) as a two-dimensional (2D) integral, which can then be numerically evaluated. With our particular problem in mind, we will follow this route.

First, notice that just after the $\ell = 1$ SPP the coherence function, given by combining Eqs. (8.2) and (8.4), assumes the form

$$W(\boldsymbol{\rho_1}, \boldsymbol{\rho_2}; 0) = A(\boldsymbol{\rho}_1) A^*(\boldsymbol{\rho}_2) f(\boldsymbol{\rho}_1 - \boldsymbol{\rho}_2), \tag{8.6}$$

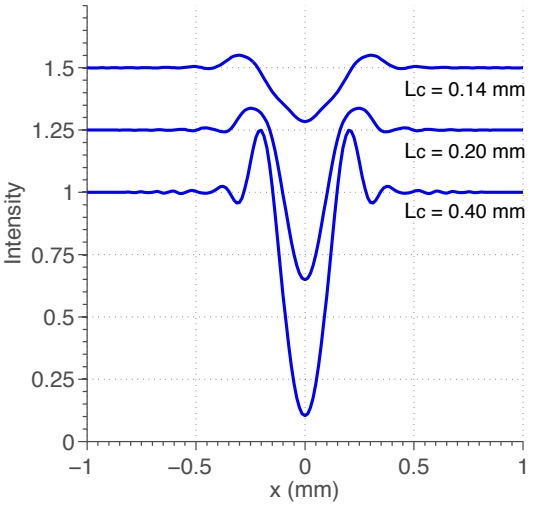

Figure 8.2: Cross sections of the theoretical (normalized) intensity distributions in the plane $z = 45$ mm for different values of the coherence length L_c at the SPP and open second aperture. The curves are vertically displaced by 0.25 from each other.

with

$$A(\boldsymbol{\rho}) = T(\rho) e^{\frac{i\pi}{\lambda L}\rho^2} e^{i\phi}, \tag{8.7}$$

$$f(\rho) = \frac{J_1(\alpha\rho)}{\alpha\rho}. \tag{8.8}$$

Equation (8.6) is very general and applies to all quasihomogeneous light sources [133]. The propagation of this coherence function to a plane $z > 0$ is given by substituting Eq. (8.6) in Eq. (8.5). By introducing "sum" and "difference" coordinates

$$\boldsymbol{\rho}_+ = \frac{\boldsymbol{\rho}_1' + \boldsymbol{\rho}_2'}{2}, \qquad \Delta\boldsymbol{\rho} = \boldsymbol{\rho}_1' - \boldsymbol{\rho}_2', \tag{8.9}$$

$$\boldsymbol{\sigma} = \frac{\boldsymbol{\rho}_1 + \boldsymbol{\rho}_2}{2}, \qquad \boldsymbol{\delta} = \boldsymbol{\rho}_1 - \boldsymbol{\rho}_2. \tag{8.10}$$

we can simplify the propagation integral to

$$W(\boldsymbol{\rho_1}, \boldsymbol{\rho_2}; z) = \int f(\Delta\boldsymbol{\rho})\, e^{-i\frac{k}{z}\Delta\boldsymbol{\rho}\cdot\boldsymbol{\sigma}} \times \tag{8.11}$$
$$\left[\int g\left(\boldsymbol{\rho}_+ + \frac{\Delta\boldsymbol{\rho}}{2}\right) g^*\left(\boldsymbol{\rho}_+ - \frac{\Delta\boldsymbol{\rho}}{2}\right)\, e^{-i\frac{k}{z}\boldsymbol{\rho}_+\cdot\boldsymbol{\delta}}\, d\boldsymbol{\rho}_+\right] d\Delta\boldsymbol{\rho},$$

where we defined the function

$$g(\boldsymbol{\rho}) \equiv A(\boldsymbol{\rho}) e^{i\frac{k}{2z}\rho^2}. \tag{8.12}$$

Next, we write the functions g and g^* in the second integral (between brackets) in terms of its Fourier transform, $G(\mathbf{u}) = \mathscr{F}[g]$. After some straightforward manipulations and simplifications one recognizes the Fourier transform $F(\mathbf{u}) = \mathscr{F}[f]$ of the function $f(\Delta\boldsymbol{\rho})$. The propagated cross-spectral density can finally be represented by the following 2D integral, instead of 4D

$$\begin{aligned} &\mathcal{W}(\boldsymbol{\sigma}, \boldsymbol{\delta}; z) = \\ &\int G\left(\mathbf{u} - \frac{k}{2z}\boldsymbol{\delta}\right) F\left(\mathbf{u} + \frac{k}{z}\boldsymbol{\sigma}\right) G^*\left(\mathbf{u} + \frac{k}{2z}\boldsymbol{\delta}\right) d\mathbf{u}. \end{aligned} \tag{8.13}$$

Equation (8.13) is represented in the sum and difference coordinates according to $\mathcal{W}(\boldsymbol{\sigma}, \boldsymbol{\delta}; z) = W(\boldsymbol{\rho_1}, \boldsymbol{\rho_2}; z)$. It allows us to compute the mutual coherence function by solving one single 2D integral for each $(\boldsymbol{\sigma}, \boldsymbol{\delta})$ combination. In practice, we are mainly interested in two important cases: the intensity distribution in the plane z, $I(\boldsymbol{\rho}; z) = W(\boldsymbol{\rho}, \boldsymbol{\rho}; z)$ which corresponds to $\boldsymbol{\sigma} = \boldsymbol{\rho}$ and $\boldsymbol{\delta} = 0$, and the "coherence" of the field $X(\boldsymbol{\rho}; z) = W(\boldsymbol{\rho}, -\boldsymbol{\rho}; z)$, which corresponds to $\boldsymbol{\sigma} = 0$ and $\boldsymbol{\delta} = 2\boldsymbol{\rho}$. From Eq. (8.13) they can be calculated via

$$I(\boldsymbol{\rho}; z) = \int |G(\mathbf{u})|^2 F\left(\mathbf{u} + \frac{k}{z}\boldsymbol{\rho}\right) d\mathbf{u}, \tag{8.14}$$

$$X(\boldsymbol{\rho}; z) = \int G\left(\mathbf{u} - \frac{k}{z}\boldsymbol{\rho}\right) F(\mathbf{u}) G^*\left(\mathbf{u} + \frac{k}{z}\boldsymbol{\rho}\right) d\mathbf{u}. \tag{8.15}$$

Equation (8.13) is especially useful if one has analytical expressions for the functions $F(\mathbf{u})$ and $G(\mathbf{u})$. A straightforward numerical integration is then able to provide the desired results. Even when such analytical expressions can't be found, Eq. (8.13) is still very convenient, since (2D) FFT algorithms for numerical Fourier transform are very efficient.

Analytical solutions can be found for our particular problem. $F(\mathbf{u})$ is the Fourier transform of the coherence term $f(\rho)$ at the plane $z = 0$, i.e.,

$$\begin{aligned} F(\mathbf{u}) = \mathscr{F}[f] &= \int \frac{J_1(\alpha|\boldsymbol{\rho}|)}{\alpha|\boldsymbol{\rho}|} e^{i\boldsymbol{\rho}\cdot\mathbf{u}}\, d\boldsymbol{\rho} \\ &= \begin{cases} 1, & u \le \frac{kd_1}{2L} \\ 0, & u > \frac{kd_1}{2L} \end{cases} \end{aligned} \tag{8.16}$$

Apart from being simple, this function conveniently limits the numerical integration to a finite range. $G(\mathbf{u})$ is the Fourier transform of the function $g(\boldsymbol{\rho})$ defined

by Eq. (8.12), which reads

$$g(\boldsymbol{\rho}) = T(\rho) e^{\frac{ik}{2}\left(\frac{1}{z}+\frac{1}{L}\right)\rho^2} e^{i\phi}, \tag{8.17}$$

where $T(\rho)$ is the intensity distribution after the second aperture. In connection with our experiments, we will assume that d_2 is very large and that the intensity is approximately uniform at $z = 0$. We have then

$$G(\mathbf{u}) = \mathscr{F}[g] = \int_0^\infty \int_0^{2\pi} \rho \; d\rho \; d\phi \; e^{ia\rho^2} e^{i(\phi + \boldsymbol{\rho}\cdot\mathbf{u})}, \tag{8.18}$$

where $a = \frac{k}{2}\left(\frac{1}{z}+\frac{1}{L}\right)$. This integral can be analytically solved and results in

$$G(\mathbf{u}) = e^{i\phi} \; u \; e^{\frac{-iu^2}{8a}} \left[J_1\left(\frac{u^2}{8a}\right) + iJ_0\left(\frac{u^2}{8a}\right)\right], \tag{8.19}$$

where ϕ is the azimuthal angle of $\mathbf{u}$ and J_0 and J_1 are the zeroth- and first-order Bessel functions. If the illumination is nonuniform but Gaussian $T(\rho) = e^{-\rho^2/w^2}$, due to partial coherence at the first aperture, the solution of Eq. (8.18) retains its form, but with the substitution $ia \to ia - 1/w^2$.

Next, we will present results for numerical calculations performed for a range of parameters similar to those used in our experiments. We consider the propagation of the coherence function to the plane $z = 45$ mm from the SPP for different values of the coherence length L_c of the beam.

Figure 8.2 shows cross sections of the calculated intensity profiles when the coherence length of the source is varied. The predictions agree with those in [147], namely, that the core of the beam behind the SPP fills with diffuse light when the coherence at the SPP is decreased. The dip in the intensity drops to zero in the limit of completely coherent illumination. The intensity for points far away from the center remains uniform and is not affected by the SPP. With partially coherent illumination, the signature of a coherence singularity is only revealed in the *coherence* of the beam.

Figure 8.3 shows cross sections of the calculated coherence $X(\boldsymbol{\rho})$ in the presence and absence of the SPP. The calculations are made using Eq. (8.15) for various values of the input coherence length L_c. The results are normalized to modulus one. For completeness, we note that a different kind of normalization is more often employed, namely, $\mu(\mathbf{r}_1, \mathbf{r}_2) = W(\mathbf{r}_1, \mathbf{r}_2)/\sqrt{I(\mathbf{r}_1)I(\mathbf{r}_2)}$. The so-called *spectral degree of coherence* μ reaches its upper bound $|\mu| = 1$ when pairs of points are completely correlated. Experimentally, however, it is more convenient to study the cross-spectral density W, instead of μ, and normalize it to some reference value.

The dashed lines show the coherence $X(\boldsymbol{\rho})$ for propagation without a phase plate. In this case we observe the coherence Airy rings, described by $J_1(x)/x$. The coherence length L_c at the plane $z = 45$ mm is slightly larger than the L_c

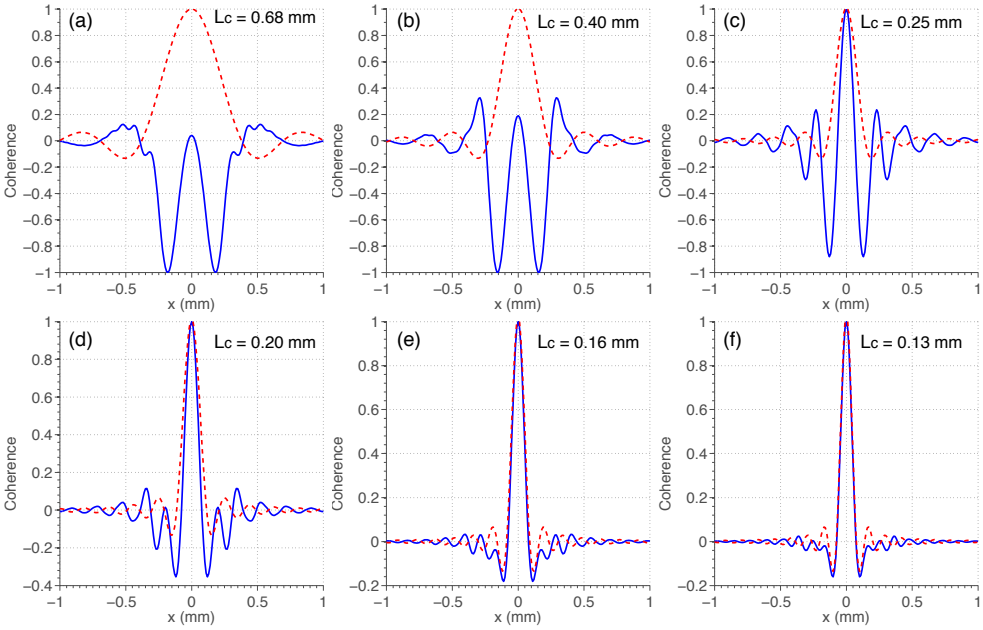

Figure 8.3: Cross sections of the theoretical coherence $X(\boldsymbol{\rho})$ of the beam in the plane $z = 45$ mm after the (open) second aperture. The dashed line is the prediction without phase plate; the continuous line corresponds to a SPP placed at aperture 2. The calculations are made for different values of the coherence length, (a) $L_c = 0.68$ mm, (b) $L_c = 0.40$ mm, (c) $L_c = 0.25$ mm, (d) $L_c = 0.20$ mm, (e) $L_c = 0.16$ mm, and (f) $L_c = 0.13$ mm.

at $z = 0$ mm. This occurs because light "gains" coherence under the additional propagation. The coherence length at the plane z can be approximated by $L_c^z \approx L_c(1 + z/L)$.

The addition of a SPP at $z = 0$ mm considerably modifies the coherence $X(\boldsymbol{\rho})$, now depicted as continuous lines. When the coherence length of the beam is relatively high, as in Figs. 8.3 (a) and (b), a coherence singularity manifest itself as a ring dislocation in $X(\boldsymbol{\rho})$, whose radius increases with decreasing coherence. This would be the only effect observable if the cross-spectral density before the SPP were described by a Gaussian function [147]. This trend changes when the input beam already has phase dislocations, associated with Airy rings. We now find that the vortex ring due to the SPP does not cross the first Airy ring when L_c is reduced, as has been hypothesized in Ref. [154], but modifies the coherence function as a whole. In fact, the presence of the SPP can even reduce the number of phase dislocations within a certain radius. For example, in Fig. 8.3(e) the coherence function without SPP crosses the zero six times for $|x| < 0.5$ mm, but only five times when the SPP is in place.

Another interesting feature concerns the relative phase of the Airy rings in

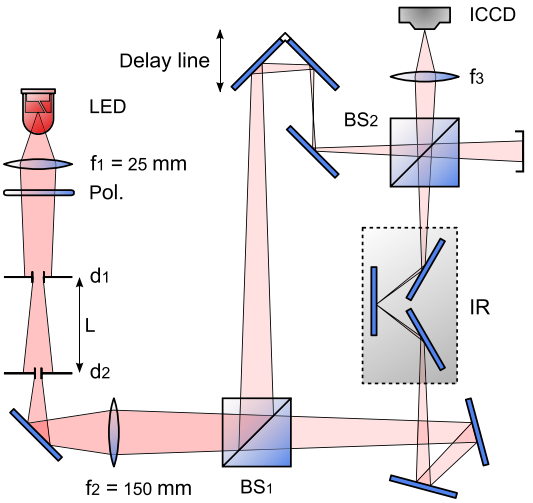

Figure 8.4: Experimental setup used to generate a partially coherent beam and to measure its mutual coherence function (see text for details).

the cases with and without SPP. For radii larger than some x_d, the phase of the Airy rings with the SPP inserted is observed to shift by π with respect to the case where the SPP is absent. The smaller the coherence length L_c, the larger x_d. For our geometry, the effect of the SPP on the coherence function is thus to shift the phase of the Airy rings by π when $|x| \to \infty$.

8.4 Measurements of the spatial coherence

The experimental determination of the mutual coherence function is a very important task in optics. Different techniques have been proposed and implemented, such as Young interferometers [163, 164] and different types of image inversion interferometers [165], like Sagnac [166–168] and Mach-Zehnder [169]. Most approaches, however, don't allow a direct visualization of the coherence function and positions and angles must be scanned to allow full reconstruction. In the following experiments, we will take advantage of our rotationally symmetric geometry and introduce a powerful method to visualize and measure the coherence function.

Figure 8.4 shows the experimental setup used to generate a partially coherent beam and to measure its mutual coherence function. A $15\times$ magnified image of a light emitting diode (LED), with central wavelength $\lambda = 826$ nm, is centered on an adjustable circular aperture of diameter d_1, after being filtered by a polarizer. We can regard this aperture as an incoherent, circular source of uniform intensity. The light propagates a distance L to a second circular aperture of fixed diameter d_2, which is approximately uniformly illuminated. The coherence length L_c of the

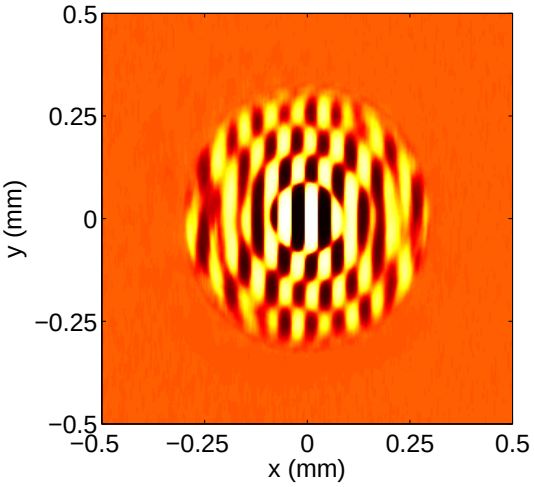

Figure 8.5: Visualization of coherence singularities in $X(\boldsymbol{\rho})$ as measured from interference fringes. The SPP is absent and the aperture 2 is imaged at the ICCD. We set $L_c = 0.15$ mm and $d_2 = 0.59$ mm. The arctangent *of X is shown in order to enhance contrast.*

light at aperture 2 can be controlled by modifying the diameter d_1 and the distance L, according to Eq. (8.3). Our results will be labeled by this coherence length, which we scan from $L_c = 0.13 - 0.68$ mm, by adjusting the first aperture in the range $d_1 = 0.6 - 3.0$ mm at $L = 200$ mm or $L = 400$ mm. A spiral phase plate (SPP) with $\ell = 1$ can be placed just after the second aperture, at an actual distance of 10 mm. We will present results with and without the SPP. Lenses are used to image the coherence function either at the plane of the second aperture, or, after some propagation, at $z = 45$ mm after the SPP. In the first case, $f_2 = 150$ mm and $f_3 = 250$ mm lenses are used to make a $4\times$ magnified image of d_2 at an intensified CCD (ICCD) camera. In the second case, $f_2 = 150$ mm and $f_3 = 40$ mm lenses are used to make a $17.7\times$ magnified image of the plane $z = 45$ mm at the ICCD.

In order to measure the mutual coherence function, the generated beam is sent through a Mach-Zehnder interferometer, where it is initially split at beam splitter BS1 and then recombined at BS2. In one of the arms of this interferometer there is an image rotator (IR), which rotates the input image by θ degrees around its axis. A delay line allows us to set both arms of the interferometer to the same length. The original beam is then recombined with a rotated version of itself, and the interference pattern is recorded with the ICCD. Following Eq. (8.1), the cross spectral density $W(\boldsymbol{\rho}_1, \boldsymbol{\rho}_2; z)$ can be obtained by measuring the interference pattern and subtracting the single intensities, which are obtained by blocking either arm of the interferometer.

The setup is ideal to extract the intensity $I(\boldsymbol{\rho})$ and the coherence $X(\boldsymbol{\rho})$ and to directly visualize the coherence singularities. The measured patterns will be rotationally symmetric when all components are properly aligned. A rotational

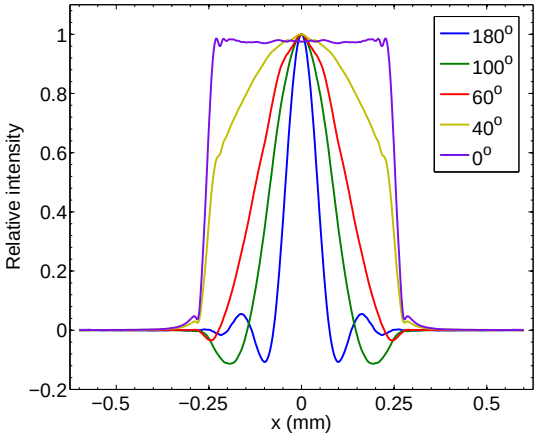

Figure 8.6: Cross sections of the interference pattern for different values of the angle of rotation θ. The coherence length of the source is $L_c = 0.15$ mm, the diameter of the second aperture is $d_2 = 0.59$ mm, and the imaged plane is $z = 0$ mm. The SPP is not in the setup.

average of the cross sections will fully characterize $I(\boldsymbol{\rho})$ or $X(\boldsymbol{\rho})$. Alternatively, a more straightforward visualization of the singularities can be obtained by misaligning beam splitter BS_2, so that interference fringes are observed. Let us first illustrate this fringes method.

Figure 8.5 shows how the singularities in the coherence $X(\boldsymbol{\rho})$ can be visualized by means of interference fringes. The SPP is absent and we choose $L_c = 0.15$ mm and $d_2 = 0.59$ mm. The plane of the aperture 2 is imaged at the ICCD. The image rotation is maximum, at $\theta = 180°$. To enhance contrast, the *arctangent* of the results is shown, while some noise is removed with a Savitzky-Golay smoothing filter [170]. For $\theta = 180°$, we are basically interfering the points $\boldsymbol{\rho}$ and $-\boldsymbol{\rho}$, to reveal the coherence of the field. The singularities related to the Airy rings are clearly visible as flips from dark to bright within a fringe line. When the separation between these points equals the coherence length L_c, the function is zero valued. For larger separations, the field fluctuations can be either correlated or anti-correlated. A π phase shift indicates a coherence singularity and the transition between correlation and anti-correlation.

Figure 8.6 shows rotationally averaged cross sections of the measured interference pattern for different rotation angles θ. These measurements are performed with the interferometer completely aligned. According to Eq. (8.2), we expect the interference to scale as

$$\mathrm{W}_0(\rho,\theta) = |T(\rho)|^2 \frac{J_1\left[\alpha(\theta)\rho\right]}{\alpha(\theta)\rho}, \tag{8.20}$$

where $\alpha(\theta) = 2\pi d_1 \sin(\theta/2)/\lambda L$. At $\theta = 0°$, we observe only the intensity distribution, which is the top-hat transmission profile of aperture 2. At $\theta = 180°$,

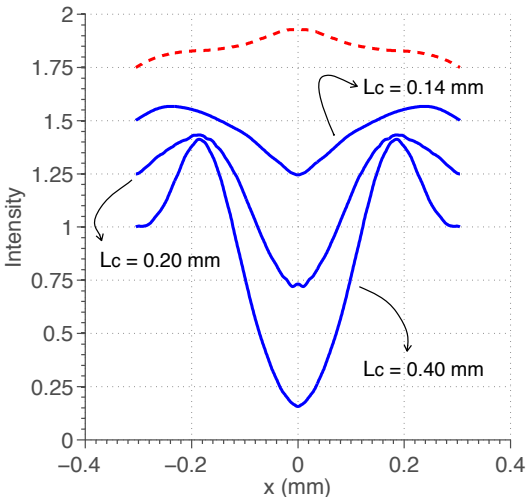

Figure 8.7: Rotationally averaged cross sections of the intensity profiles in the plane $z = 45$ mm after the SPP. The dashed curve shows the intensity profile in the absence of the SPP. All curves are normalized and are displaced by 0.25 from each other.

we observe the coherence of the field. Most noticeable, a rotation from $180°$ to $0°$ allows one to "zoom in" the (central structure) of the coherence, of which the horizontal axis scale as $1/\alpha(\theta)$. Notice how the coherence is strechted as θ decreases.

Figures 8.7-8.9 present results of measurements performed when a $\ell = 1$ SPP is placed just after the second aperture. As discussed in Section 8.2, prominent effects are expected to be observed only after propagation. In the following experiments, the second aperture is wide open at $d_2 = 2$ mm and the plane $z = 45$ mm is imaged on the ICCD. A magnification of $17.7\times$ is used in order to highlight the effects close to the beam center.

Figure 8.7 shows measurements of the intensity $I(\boldsymbol{\rho})$ for different values of the coherence length L_c at the SPP. The curves are rotationally averaged cross sections of the intensity profiles measured by the ICCD. The observed intensity dips are similar to those reported in [147] and in agreement with our calculations and Fig. 8.2. The dips are more prominent when the coherence length is large; the dark core is filled with diffuse light at reduced L_c. Furthermore, the maximum in the intensity is closer to the center at large coherence ($L_c = 0.40$) than at small coherence ($L_c = 0.14$). The dashed curve shows the intensity profile without SPP; it varies just slightly in the considered range.

Figure 8.8 shows the coherence $X(\boldsymbol{\rho})$ measured in the plane $z = 45$ mm for different coherence lengths L_c of the illumination. The rotationally averaged cross-sections are displayed on the left (dashed curve without the SPP, solid curve with SPP). The interference fringes made with beamsplitter BS_2 misaligned are

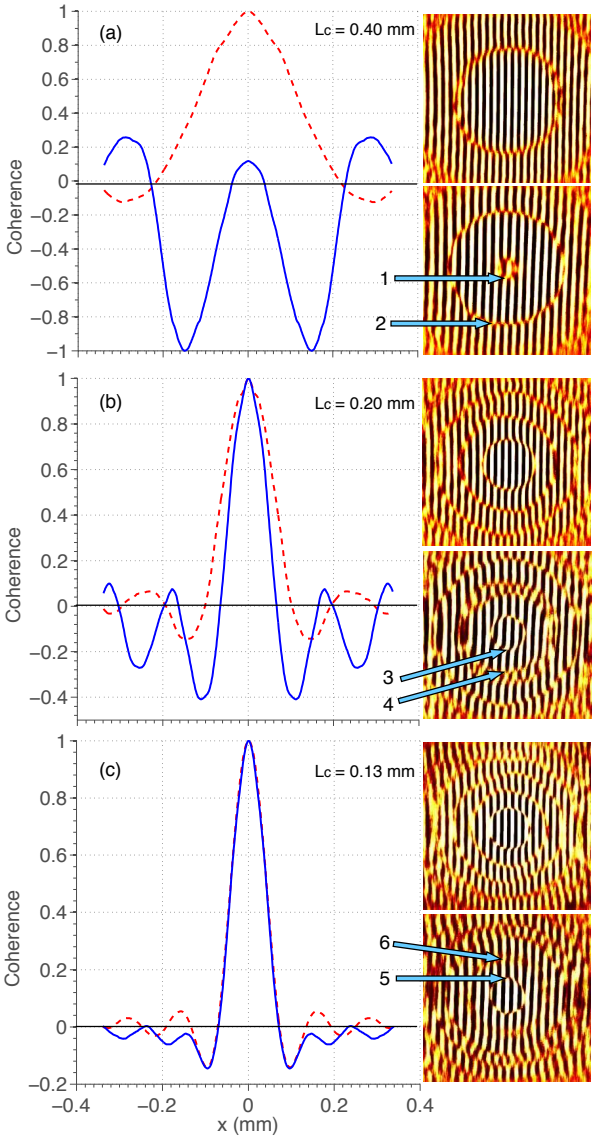

Figure 8.8: Measured coherence $X(\boldsymbol{\rho})$ for (a) $L_c = 0.40$ mm, (b) $L_c = 0.20$ mm, and (c) $L_c = 0.13$ mm. Left column*: rotationally averaged cross sections. Continuous curves are measured with the SPP; dashed curves are without SPP.* Right column*: Interference patterns measured with beam splitter BS_2 misaligned. Upper figures correspond to the case without SPP and lower figures to the case with SPP.*

shown on the right (top pictures without SPP, bottom pictures with SPP). All the results are normalized to modulus one.

Figure 8.8(a) shows that when the coherence length is relatively large ($L_c = 0.40$ mm), the effect of the SPP is to create an additional small ring dislocation in the coherence $X(\boldsymbol{\rho})$, indicated by arrow 1. The second dislocation, associated with the Airy ring, is pushed slightly outwards (arrow 2). Two phase jumps are clearly observable by following a fringe that goes through the center of the pattern. Notice also that the phase of the Airy rings are π-shifted with respect to the case without SPP. Figure 8.8(b) shows that as the coherence of the source decreases, the radius of the vortex ring increases (arrow 3), up to a point where it approaches the shrinking Airy rings (arrow 4).

Figure 8.8(c) shows the measured coherence $X(\boldsymbol{\rho})$ at $L_c = 0.13$ mm. At this point, the first singularity with the SPP already coincides with the first Airy ring in the coherence without SPP (arrow 5). The effect of the SPP is now far from trivial, but one can clearly see that it does reduce the total number of phase jumps, with respect to the case where the SPP is present. This is nicely illustrated in the fringes patterns. Notice that, contrary to Figs. 8.8(a) and 8.8(b), in Fig. 8.8(c) the fringes for the measurement with the SPP flip one time less than for the measurements without the SPP. There are no phase jumps at the position shown by arrow 6. It is also clear in the cross section that the coherence $X(\boldsymbol{\rho})$ approaches the zero axis, but doesn't cross it. In the comparison of $X(\boldsymbol{\rho})$ with and without SPP in Fig. 8.8(c), we distinguish three regimes. For $\rho \lesssim 0.14$ mm the coherence for the case with SPP coincides with the one for the case without SPP. For $\rho \gtrsim 0.25$ mm these two functions approximately coincide, but are π-shifted from each other; and for 0.14 mm $\lesssim \rho \lesssim 0.25$ mm, there is a transition region. All measurements are in good agreement with the theoretical predictions shown in Fig. 8.3.

Finally, we have tracked how the first ring dislocation depends on the coherence length L_c of the beam. Figure 8.9 shows the diameter D of the first zero of the coherence $X(\boldsymbol{\rho})$ as function of L_c. Two regimes can be distinguished. When L_c is relatively large, D increases with decreasing L_c. When the mutual coherence before the SPP is described by a Gauss-Schell model, one expects [154]

$$D = \sqrt{\frac{2}{\pi}} \frac{z\lambda}{L_c}. \tag{8.21}$$

In our experiments, we expect then a dependence $D = 0.030/L_c$. A curve fitting using only the last eight points of the plot provide $D = (0.027 \pm 0.001)/L_c$ mm, which is in reasonably good agreement. The other regime occurs for smaller values of L_c. In this regime the first zero of $X(\boldsymbol{\rho})$ coincides with the Airy ring. Since the first zero of the Airy ring is our definition of coherence length, we now expect $D = L_c$. This line is also shown in the plot.

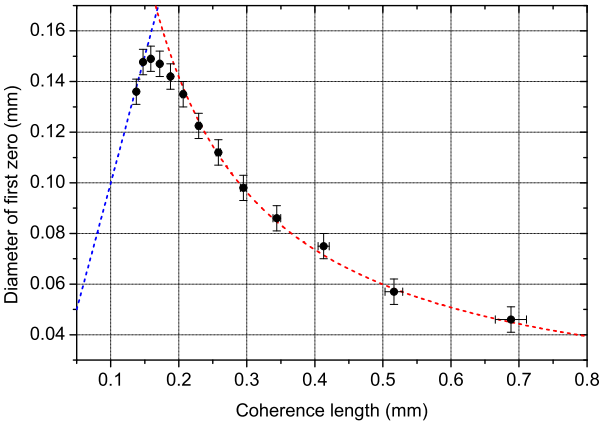

Figure 8.9: Dependence of the diameter of the first dislocation ring on the coherence length L_c of the input beam. The left line is defined as $D = L_c$. The right curve is a curve fit of the last eight points and has the form $D = (0.027 \pm 0.001)/L_c$.

8.5 Conclusion

In this Chapter we implement a method to directly visualize the coherence function of beams with two types of coherence singularities, Airy rings and a coherence vortex created by a spiral phase plate (SPP). As long as the radius of this vortex ring is small compared to the first Airy ring, the general features can be explained by the model presented in [147], which assumes a Gaussian shape for the coherence. In this regime, the origin of the coherence singularity can be well understood from a geometrical optics point of view, as discussed in [152]. For smaller values of the coherence length L_c, the presence of the SPP modifies the coherence function in a more subtle way. A clear-cut physical picture of the interaction between the Airy rings and the coherence vortex is not available. We formulate a theoretical description of the problem and present numerical simulations. Experimental and theoretical results are in good agreement. Curiously and non intuitively, the phase plate can reduce the total number of phase singularities in the field, instead of increasing it. Furthermore, the SPP shifts the phase of the Airy rings by π, for larger radii. These results provide new insights into the spatial coherence of beams with non-zero overall orbital angular momentum and into the properties of spatial correlation vortices.